

Manipulating nonequilibrium magnetism through superconductors

Francesco Giazotto,* Fabio Taddei, Rosario Fazio, and Fabio Beltram
NEST-INFM and Scuola Normale Superiore, I-56126 Pisa, Italy

Electrostatic control of the magnetization of a normal mesoscopic conductor is analyzed in a hybrid superconductor-normal-superconductor system. This effect stems from the interplay between the non-equilibrium condition in the normal region and the Zeeman splitting of the quasiparticle density of states of the superconductor subjected to a static in-plane magnetic field. Unexpected spin-dependent effects such as magnetization suppression, *diamagnetic-like* response of the susceptibility as well as spin-polarized current generation are the most remarkable features presented. The impact of scattering events is evaluated and let us show that this effect is compatible with realistic material properties and fabrication techniques.

PACS numbers: 73.20.-r, 73.23.-b, 75.75.+a

The interplay between out-of-equilibrium transport and superconductivity [1] was recently successfully exploited in a number of systems in order to implement Josephson transistors [2, 3, 4], π junctions [5] and electron microrefrigerators [6, 7], just to mention a few relevant examples. In this Letter we explore its potential in the area of magnetism [8] and spintronics [9] and present a novel approach to control the magnetization and spin-dependent properties of a mesoscopic normal conductor. In particular, we show that manipulation of the (nonequilibrium) distribution of a normal metal through an applied voltage can lead to the control of a number of spin-dependent phenomena. The key ingredients are superconductor electrodes (with energy gap Δ) and a weak external magnetic field. The resulting Zeeman-split superconductor density of states (DOS) was originally exploited by Tedrow and Meservey to measure the spin-polarization of ferromagnets in the case of Al electrodes [10]. As we shall argue, the interplay between Zeeman splitting and nonequilibrium yields dramatic consequences on quasiparticle dynamics stemming from the peculiar shape of the superconductor DOS whose energy gap compares well with magnetic fields readily accessible experimentally.

Let us consider the system sketched in Fig. 1. It consists of two superconducting reservoirs (S) connected by a mesoscopic normal metal wire (N) through tunnel contacts (I) of resistance R_I . The structure is biased at a voltage V_C and in the presence of a static in-plane magnetic field H , applied either across the whole structure (Fig. 1(a), in the following referred to as **a-type** setup) or localized at the superconductors (Fig. 1(b), **b-type** setup). For the sake of simplicity let us assume a symmetric structure (a resistance asymmetry would not change the overall physical picture). As for the superconductors we focus on conventional low critical-temperature thin (< 10 nm) films. In this case the effect of H on the electron spin becomes dominant and, assuming negligible spin-orbit interaction [11], the superconductor DOS per spin is

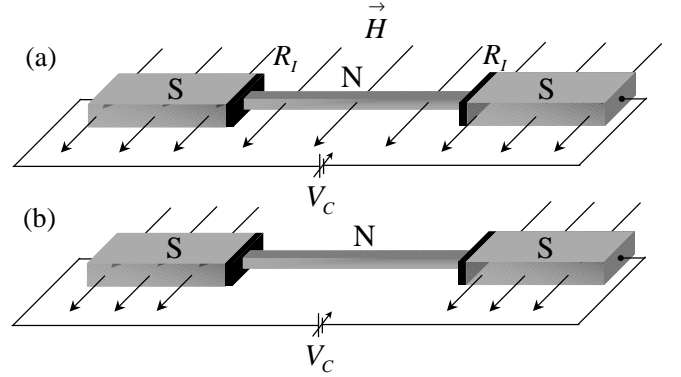


FIG. 1: Scheme of the structure investigated. An in-plane static magnetic field H is applied across the whole SINIS system ((a), **a-type** setup) or localized at the S electrodes ((b), **b-type** setup). A finite voltage bias V_C drives the normal metal out-of-equilibrium allowing to control its magnetization. The N wire is assumed quasi-one-dimensional.

BCS-like but shifted by the Zeeman energy ($E_H = \mu_B H$), $\mathcal{N}_\sigma^S(\varepsilon) = \mathcal{N}_F^N |\text{Re}[(\varepsilon + \sigma E_H)/2\sqrt{(\varepsilon + \sigma E_H)^2 - \Delta^2}]|$ [12], where ε is the quasiparticle excitation energy measured from the Fermi energy (ε_F), \mathcal{N}_F^N is the DOS in the normal state at ε_F (2 spin directions), μ_B is the Bohr magneton, and $\sigma = \pm 1$ refers to spin parallel(antiparallel) to the field.

At a finite bias V_C , in the presence of H and in the limit of negligible inelastic collisions, the steady-state distribution functions in the metal wire are spin-dependent and are given by [13]

$$f_\sigma(\varepsilon, V_C, H) = \frac{\mathcal{N}_\sigma^L \mathcal{F}^L + \mathcal{N}_\sigma^R \mathcal{F}^R}{\mathcal{N}_\sigma^L + \mathcal{N}_\sigma^R}, \quad (1)$$

where $\mathcal{F}^{L(R)} = f_0(\varepsilon \pm eV_C/2)$, $\mathcal{N}_\sigma^L = \mathcal{N}_\sigma^S(\varepsilon + eV_C/2)$, $\mathcal{N}_\sigma^R = \mathcal{N}_\sigma^S(\varepsilon - eV_C/2)$, $f_0(\varepsilon)$ is the Fermi distribution at lattice temperature T and e is the electron charge. Owing to the nonequilibrium regime driven by the applied electric field, the quasiparticle distributions corresponding to different spin species behave differently, $f_{+(-)}$ being shifted towards lower(higher) energy. The magnetic

*Electronic address: giazotto@sns.it

properties of the N region are entirely determined by its (spin-dependent) quasiparticle distribution functions. The magnetization density in the wire is indeed given by

$$\mathcal{M}(V_C, H) = \mu_B \int d\varepsilon [\mathcal{N}_+^N(\varepsilon) f_+(\varepsilon) - \mathcal{N}_-^N(\varepsilon) f_-(\varepsilon)], \quad (2)$$

where $\mathcal{N}_\sigma^N(\varepsilon) = \frac{1}{2} \mathcal{N}^N(\varepsilon_F + \varepsilon + \sigma \mu_B H)$ and $\mathcal{N}^N(\varepsilon)$ is the N region DOS in the absence of magnetic field. The function $\mathcal{M}(V_C, H)$ vs V_C is displayed in Fig. 2(a,b) for different magnetic-field values. We assumed a silver (Ag) N region (with $\mathcal{N}_F^N = 1.03 \times 10^{47} \text{ J}^{-1} \text{ m}^{-3}$) at temperature $T = 0.1 T_c$, where $T_c = (1.76 k_B)^{-1} \Delta = 1.196 \text{ K}$ is the critical temperature of bulk aluminum (Al, the material forming the S regions) and k_B is the Boltzmann constant. When H is applied across the whole SINIS structure (**a**-type setup), \mathcal{M} decreases upon increasing V_C starting from its equilibrium value $\mathcal{M}_{Pauli} = \mu_B^2 \mathcal{N}_F^N H$ typical of a Pauli paramagnet [8] (see Fig. 2(a)). \mathcal{M} shows a complete suppression for $V_C \gtrsim \Delta/e$, i.e. the N region is *demagnetized*. The inset of Fig. 2(a) shows how $\mathcal{M}(V_C)$ is weakly dependent on the lattice temperature up to $T = 0.4 T_c$ owing to the BCS $\Delta(T)$ dependence together with the temperature-induced broadening of $f_0(\varepsilon)$. Conversely, when the magnetic field is localized at the S electrodes (**b**-type setup) a *negative* magnetization is induced in the wire (see Fig. 2(b)). Note that \mathcal{M} is antiparallel to H . Therefore, the N region behaves as a "diamagnet" [14]. For $eV_C \gtrsim \Delta$ the wire susceptibility χ (shown in Fig. 1(c) at $T = 0.1 T_c$) reaches the Pauli value but with opposite sign $\chi = \partial \mathcal{M} / \partial H = -\mu_B^2 \mathcal{N}_F^N = -\chi_{Pauli}$. This gives rise to a sort of "artificial" Pauli diamagnetism.

Insight into the physical origin of this superconductivity-controlled magnetism can be qualitatively gained by considering the (zero-temperature) steady-state DOS diagrams of Fig. 2(a',b'), where the normal metal is described by parabolic subbands typical of a free electronlike paramagnetic conductor such as silver. At *equilibrium* the occupation of quasiparticle states is identical for both spin species leading to $\mathcal{M} = \mathcal{M}_{Pauli}$ and $\mathcal{M} = 0$ for **a**-type and **b**-type setups, respectively. When $V_C \neq 0$, electron distributions for the two spin populations are characterized by distinct chemical potentials μ^σ . Since $\mu^+ < \mu^-$ the occupation of spin states antiparallel to the magnetic field is favored with respect to the parallel one, owing to the opposite energy shift of the superconductor spin-dependent DOS in the external magnetic field. This leads to a reduction of \mathcal{M} for the **a**-type setup and to negative magnetization for the **b**-type setup. In particular, at $V_C \sim \Delta/e$ the chemical potential separation is $\delta\mu = \mu^+ - \mu^- \sim -2\mu_B H$ for both setups. This shows a full *electrostatic* control of the magnetization, a unique feature of the present system [15]. The superconducting reservoirs are *essential* elements for these effects to be present and replacing them by ordinary normal contacts would only always lead to a negligible paramagnetic correction to the actual \mathcal{M} (second order in the small quantities $\mu_B H / \varepsilon_F$ and

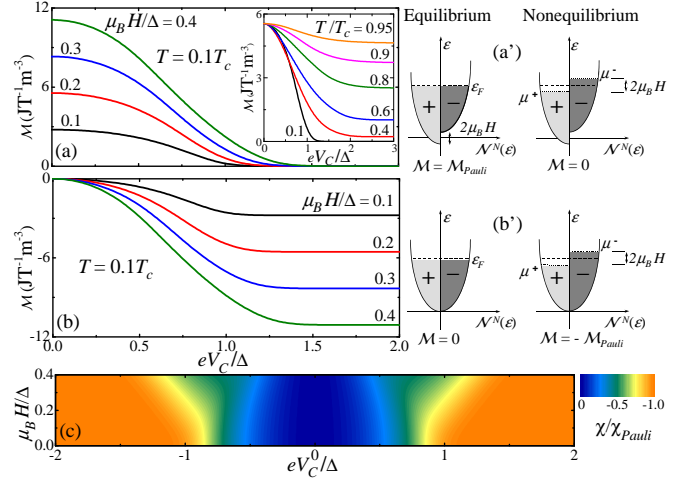


FIG. 2: (color) (a) Magnetization density \mathcal{M} vs bias voltage V_C at $T = 0.1 T_c$ for different magnetic fields (H) for **a**-type setup (see Fig. 1(a)). Inset: \mathcal{M} vs V_C for different temperatures at $H = 0.2 \Delta/\mu_B$. (b) The same as in (a) for **b**-type setup. (a') Schematic diagrams of the N region density of states and quasiparticle occupation both at equilibrium (left) and nonequilibrium (right) for **a**-type setup. (b') The same as in (a') for **b**-type setup. (c) Contour plot of the normalized magnetic susceptibility χ/χ_{Pauli} vs V_C and H at $T = 0.1 T_c$ for **b**-type setup.

eV_C/ε_F).

The experimental accessibility of this operational principle must be carefully assessed. Electrons in metals experience both elastic and inelastic collisions. The latter drive the system to equilibrium and can be expected to hinder the observation of the phenomena discussed here. Our analysis will show a remarkable robustness of these effects. At low temperatures (typically below 1 K) electron-electron scattering [16], and scattering with magnetic impurities [17, 18] are the dominant sources of inelastic collisions [18, 19, 20]. Since R_I is in general large compared to wire resistance ($R_N = L/\mathcal{N}_F^N e^2 D A$, where L is the length, A the cross-section and D the wire diffusion constant), we can assume that f_σ changes only at the interfaces, being essentially constant elsewhere [21]. The effect of electron-electron scattering due to direct Coulomb interaction on the spin-dependent distributions can be accounted for by solving a pair of coupled stationary kinetic equations:

$$\begin{cases} D \frac{\partial^2 f_+(\varepsilon)}{\partial x^2} = \mathcal{I}_{\text{coll}}^+(\varepsilon) \\ D \frac{\partial^2 f_-(\varepsilon)}{\partial x^2} = \mathcal{I}_{\text{coll}}^-(\varepsilon), \end{cases} \quad (3)$$

together with the Kuprianov-Lukichev boundary conditions at the NIS interfaces [22]. In (3) $\mathcal{I}_{\text{coll}}^\sigma(\varepsilon)$ is the net collision rate at energy ε , functional of the distributions functions f_σ , defined by

$$\mathcal{I}_{\text{coll}}^\sigma(\varepsilon) = \mathcal{I}_{\text{coll}}^{\text{in}\sigma}(\varepsilon) - \mathcal{I}_{\text{coll}}^{\text{out}\sigma}(\varepsilon), \quad (4)$$

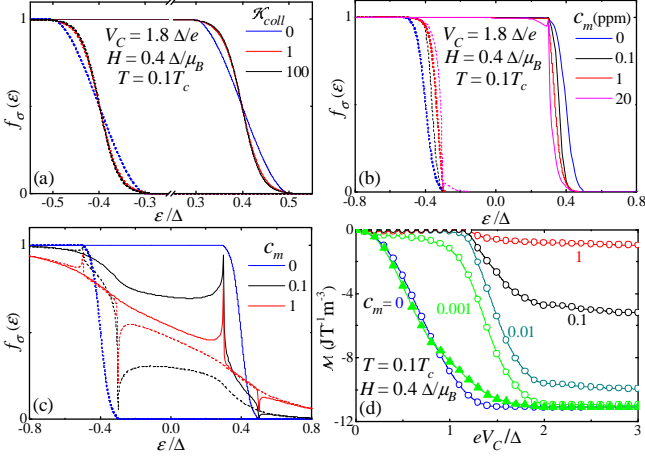


FIG. 3: (color) (a) Spin-dependent distribution functions $f_\sigma(\epsilon)$ vs energy ϵ calculated for three \mathcal{K}_{coll} values at $H = 0.4 \Delta/\mu_B$, $V_C = 1.8 \Delta/e$ and $T = 0.1 T_c$. Solid(dashed) lines correspond to antiparallel(parallel) spin species. (b) $f_\sigma(\epsilon)$ vs ϵ calculated for various c_m values at $H = 0.4 \Delta/\mu_B$, $V_C = 1.8 \Delta/e$ and $T = 0.1 T_c$ for **a**-type setup. (c) The same as in (b) for **b**-type setup. (d) Magnetization density \mathcal{M} vs V_C at $H = 0.4 \Delta/\mu_B$ and $T = 0.1 T_c$ for different magnetic impurity concentration. Open circles refer to **b**-type setup, filled triangles to **a**-type setup for $c_m = 0.001$. The latter were shifted by $-\mathcal{M}_{Pauli}$. Data in (b)-(d) were obtained assuming $D = 0.02 \text{ m}^2\text{s}^{-1}$, $T_K = 40 \text{ mK}$ and $S = \frac{1}{2}$.

where

$$\mathcal{I}_{coll}^{in\sigma}(\epsilon) = [1 - f_\sigma(\epsilon)] \int d\omega \frac{k(\omega)}{2} f_\sigma(\epsilon - \omega) \int dE \{f_+(E + \omega)[1 - f_+(E)] + f_-(E + \omega)[1 - f_-(E)]\} \quad (5)$$

and

$$\mathcal{I}_{coll}^{out\sigma}(\epsilon) = f_\sigma(\epsilon) \int d\omega \frac{k(\omega)}{2} [1 - f_\sigma(\epsilon - \omega)] \int dE \{f_+(E)[1 - f_+(E + \omega)] + f_-(E)[1 - f_-(E + \omega)]\}. \quad (6)$$

In (5) and (6), $k(\omega) = \kappa_{ee}\omega^{-3/2}$ according to the theory of screened Coulomb interaction [23] for a quasi-one dimensional wire, where $\kappa_{ee} = (\pi\sqrt{2D}\hbar^{3/2}\mathcal{N}_F^N A)^{-1}$ [24, 25]. By making (3) dimensionless [21], the strength of the electron-electron interaction can then be expressed as $\mathcal{K}_{coll} = (R_I/R_N)(L^2\kappa_{ee}/D)\sqrt{\Delta} = (L/\sqrt{2})(R_I/R_K)\sqrt{\Delta/\hbar D}$, where $R_K = h/2e^2$.

We analyzed quantitatively a realistic Ag/Al SINIS microstructure [6, 7] with $L = 1 \mu\text{m}$, $A = 0.2 \times 0.02 \mu\text{m}^2$, and $R_I = 10^3 \Omega$. Figure 3(a) illustrates the effect of electron-electron scattering. We solved (3) with $H = 0.4 \Delta/\mu_B$, $V_C = 1.8 \Delta/e$ and $T = 0.1 T_c$ for several \mathcal{K}_{coll}

values from negligible ($\mathcal{K}_{coll} = 0$, blue lines), to moderate ($\mathcal{K}_{coll} = 1$, red lines) and extreme ($\mathcal{K}_{coll} = 100$, black lines) [23, 24]. As expected, electron-electron interactions have virtually no impact. By increasing the strength of Coulomb interaction the quasiparticle distribution of each spin species relaxes toward spin-dependent Fermi functions still characterized by different chemical potentials (a similar effect is expected in the presence of interaction with the lattice phonons [26]). As a result the nonequilibrium magnetization in the normal wire here presented is virtually unaffected.

The situation drastically changes if we assume the presence of magnetic impurities in the N region, due to the resulting spin-flip processes. Above the Kondo temperature (T_K), the distribution functions can be calculated including, in the right-hand-side of Eqs. (3), an additional term derived by generalizing the theory developed by Göppert and Grabert in Ref. [27]. It is noteworthy to mention that its strength is proportional, apart from the electron and magnetic impurity spin coupling constant, to the *total* number of magnetic impurities present within the wire (i.e., to the product $c_m LA$, with c_m the impurity concentration) and R_I . The resulting distribution functions relative to the **a**-type setup are shown in Fig. 3(b) at $H = 0.4 \Delta/\mu_B$, $V_C = 1.8 \Delta/e$ and $T = 0.1 T_c \approx 120 \text{ mK}$ for various c_m values expressed in parts per million (ppm). We assumed $D = 0.02 \text{ m}^2\text{s}^{-1}$ (typical of high-purity Ag), magnetic impurities with spin $S = \frac{1}{2}$, and $T_K = 40 \text{ mK}$ (as appropriate, for example, for Mn impurities in Ag) [29, 30]. By increasing c_m , examination of the figure immediately shows that spin-dependent distributions are marginally affected even for impurity concentrations as large as 20 ppm. This shows that in the **a**-type setup the nonequilibrium \mathcal{M} is relatively *insensitive* to large amounts of magnetic impurities. Figure 3(c) shows the $f_\sigma(\epsilon)$ calculated for various c_m values for the **b**-type setup. In such a case, by contrast, the spin-dependent distribution functions tend to merge for much lower values of c_m thus suppressing the induced magnetization. In the presence of a magnetic field across the N region (**a**-type setup) impurity spins tend to polarize yielding a suppression of spin-flip relaxation processes for the field intensities of interest here [17, 18, 27, 28]. This does not occur in the **b**-type setup and makes magnetic impurities more effective in mixing spins. The full behavior of $\mathcal{M}(V_C)$ for **b**-type setup at $T = 0.1 T_c$ and $H = 0.4 \Delta/\mu_B$ is displayed in Fig. 3(d) for several c_m values (open circles). For comparison, $\mathcal{M}(V_C)$ for **a**-type setup (filled triangles) is shown at low impurity concentration. We wish to underline the robustness of the induced magnetization, \mathcal{M} being suppressed only for rather large concentrations: the latter can in fact be limited to less than 0.01 ppm in currently available high-purity metals [30].

These results on the robustness of these effects in realistic structures make it appropriate to investigate their potential for device implementation. An immediate area of application is *spintronics* [9]. Let us consider a microstructure like that shown in Fig. 4(a), where a nor-

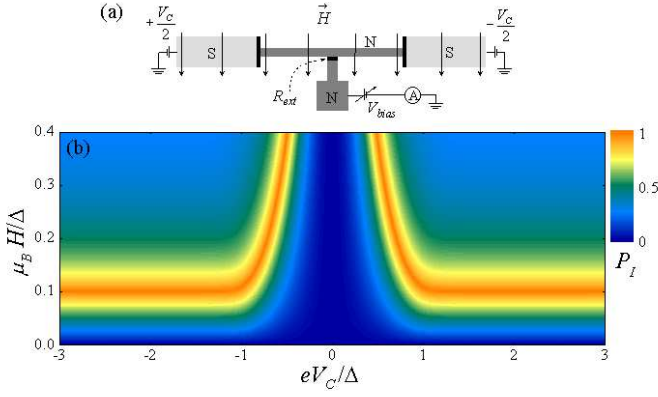


FIG. 4: (color) (a) Scheme of the spin-polarized current source in the presence of a uniform H . Spin-polarized current can be extracted by biasing the middle terminal with V_{bias} . (b) Contour plot of the nonequilibrium current polarization P_I vs V_C and H for $V_{bias} = 0.1 \Delta/e$ at $T = 0.1 T_c$.

mal "probe" terminal is tunnel-coupled to the wire [31]. Upon voltage biasing with V_{bias} , the presence of spin-dependent distributions in the N region yields a finite current polarization P_I defined as

$$P_I(V_C, H, V_{bias}) = \frac{|I_-| - |I_+|}{|I_-| + |I_+|}, \quad (7)$$

where

$$I_\sigma(V_C, H, V_{bias}) = \varphi \int d\varepsilon \mathcal{N}_\sigma^N(\varepsilon) \mathcal{N}_\sigma^N(\varepsilon + eV_{bias}) \times [f_\sigma(\varepsilon, V_C, H) - f_0(\varepsilon + eV_{bias})] \quad (8)$$

is the spin-dependent current flowing through the additional terminal. Furthermore, $\varphi = [2e(\mathcal{N}_F^N)^2 R_{ext}]^{-1}$ and

$R_{ext} \gg R_I$ is the probe junction resistance. The calculated nonequilibrium P_I is displayed in Fig. 4(b) for $T = 0.1 T_c$ and $V_{bias} = 0.1 \Delta/e$ as a function of V_C and H . We emphasize that for easily attainable values of V_C and H a 100% spin-polarized current consisting of the *antiparallel* spin species can be achieved. A quantitative estimate for realistic parameters shows that sizable spin-polarized currents can be available. For example, assuming $R_{ext} = 10^4 \Omega$ at $T = 0.1 T_c \approx 120$ mK and for an external field of 1.5 T the fully spin-polarized current reaches values up to about 10^{-8} A. We stress that P_I values largely exceed 50% over a wide region in the (V_C, H) plane. Note that at equilibrium by placing the wire in external magnetic fields of comparable intensity only values of P_I of the order of $10^{-6} \div 10^{-5}$ would be obtained.

In conclusion, we have presented a scheme to control the magnetic properties of a mesoscopic metal. Magnetism suppression as well as artificial Pauli diamagnetism can be accessed in metal-superconductor microstructures thus making available a number of characteristics of much relevance in light of possible applications: (1) Generation of 100% spin-polarized currents without invoking the use of magnetic materials; (2) *full-electrostatic* control of magnetization over complex nanostructured metallic arrays for enhanced performance and optimized device geometries; (3) reduced power dissipation ($10^{-14} \div 10^{-11}$ W depending on the control voltage) owing to the very small driving currents intrinsic to SIN junctions; (4) high magnetization switching frequencies up to 10^{11} Hz [21]; (5) ease of fabrication that can take advantage of the well-established metal-based tunnel junction technology.

This work was supported in part by MIUR under FIRB "Nanotechnologies and nanodevices for information society" contract RBNE01FSWY and by RTN-Spintronics.

-
- [1] *Theory of Nonequilibrium Superconductivity*, edited by N. B. Kopnin (Clarendon Press, Oxford, 2001).
 - [2] A.F. Morpurgo, T. M. Klapwijk, and B. J. van Wees, Appl. Phys. Lett. **72**, 966 (1998).
 - [3] A. M. Savin *et al.*, Appl. Phys. Lett. **84**, 4179 (2004).
 - [4] F. Giazotto *et al.*, Appl. Phys. Lett. **83**, 2877 (2003).
 - [5] J. J. A. Baselmans *et al.*, Nature **397**, 43 (1999).
 - [6] See J. P. Pekola, R. Schoelkopf, and J. Ullom, Phys. Today **57**, 41 (2004), and references therein.
 - [7] J. P. Pekola *et al.*, Phys. Rev. Lett. **92**, 056804 (2004).
 - [8] K. Yosida, *Theory of Magnetism*, Springer Series in Solid-State Sciences, Vol. 122 (Springer-Verlag, Berlin, 1996).
 - [9] I. Zutic, J. Fabian, S. Das Sarma, Rev. Mod. Phys. **76**, 323 (2004); G. A. Prinz, Science **282**, 1660 (1998); S. A. Wolf *et al.*, *ibid.* **294**, 1488 (2001).
 - [10] R. Meservey and P. M. Tedrow, Phys. Rep. **238**, 173 (1994).
 - [11] P. M. Tedrow and R. Meservey, Phys. Rev. Lett. **27**, 919 (1971).
 - [12] R. Meservey, P. M. Tedrow, and P. Fulde, Phys. Rev. Lett. **25**, 1270 (1970).
 - [13] D. R. Heslinga and T. M. Klapwijk, Phys. Rev. B **47**, 5157 (1993).
 - [14] It is worth mentioning that the induced magnetization vanishes if the external fields acting on the two superconductors are arranged antiparallel with each other.
 - [15] Note that one superconducting electrode is sufficient in order to control the wire magnetization.
 - [16] B. L. Altshuler and A. G. Aronov, in *Electron-Electron Interactions in Disordered Systems*, edited by A. L. Efros and M. Pollak (Elsevier, Amsterdam, 1985).
 - [17] A. Kaminski and L. I. Glazman, Phys. Rev. Lett. **86**, 2400 (2001).
 - [18] A. Anthore *et al.*, Phys. Rev. Lett. **90**, 076806 (2003).
 - [19] H. Pothier *et al.*, Phys. Rev. Lett. **79**, 3490 (1997).
 - [20] K. E. Nagaev, Phys. Rev. B **52**, 4740 (1995).
 - [21] F. Giazotto *et al.*, Phys. Rev. Lett. **92**, 137001 (2004).
 - [22] M. Yu. Kuprianov and V. F. Lukichev, Zh. Eksp. Teor.

- Fiz. **94**, 139 (1988) [Sov. Phys. JETP **67**, 1163 (1988)].
- [23] B. L. Altshuler and A. G. Aronov, Zh. Eksp. Teor. Fiz. **75**, 1610 (1978) [Sov. Phys. JETP **48**, 812 (1978)].
 - [24] A. Kamenev and A. Andreev, Phys. Rev. B **60**, 2218 (1999).
 - [25] B. Huard *et al.*, Solid State Commun. **131**, 599 (2004).
 - [26] M. L. Roukes *et al.*, Phys. Rev. Lett. **55**, 422 (1985).
 - [27] G. Göppert and H. Grabert, Phys. Rev. B **68**, 193301 (2003).
 - [28] G. Göppert *et al.*, Phys. Rev. B **66**, 195328 (2002).
 - [29] D. K. Wohlleben and B. R. Coles, *Magnetism*, vol. 5 (ed. H. Suhl) (Academic, New York, 1973).
 - [30] F. Pierre *et al.*, Phys. Rev. B **68**, 085413 (2003).
 - [31] A similar scheme would also allow an accurate determination of $f_\sigma(\varepsilon)$ from the voltage-dependent differential conductance of the probe junction [18].